Bias Correction of Satellite Data at NCEP

Paul van Delst[1], John Derber[2], Russ Treadon[2], Kozo Okamoto[3] and Wan-Shu Wu[2]

[1]CIMSS @ NOAA/NWS/NCEP/EMC,
[2]NOAA/NWS/NCEP/EMC
[3]JMA visiting scientist @ NOAA/NWS/NCEP/EMC

1. Introduction

The bias correction of satellite radiances is important for enhancing the impact on forecast skill. This paper will detail the current method of satellite data bias correction in the NCEP Global Data Assimilation System (GDAS). Areas of investigation for improving the NCEP satellite data bias correction scheme will be briefly discussed based on the sources of the biases.

2. Bias Correction Scheme

The current bias correction scheme employed in the NCEP GDAS is detailed in Okamoto and Derber (2005). The bias correction in the GDAS consists of a slowly varying component and an air mass dependent component. The bias, b, for channel j is given by,

$$b_j = s_{jm} + \sum_{k=1}^{5} c_{jk} p_{jk}$$

The slowly varying component, s_{jm}, (also referred to as the fixed angle component) is intended to remove the bias across a scan. It is computed at each scan position m from quality controlled observed minus guess (O-G) brightness temperature fields accumulated over the last 30 days, updated at every post-analysis step. A time series of the fixed angle bias correction for NOAA-16 AMSU-A channels 1, 2, 3, and 15 is shown in Figure 1 (other instruments, both infrared and microwave show similar behaviour). This bias component is very stable with time and the only significant changes occur when there are GDAS updates (as occurred on Nov. 29) or if there is an anomaly with the instrument.

The second bias component is an air mass dependent bias correction and it is expressed as a linear equation with five predictors, p_{jk}. The predictor coefficients, c_{jk}, are included as analysis variables and are determined globally. The current set of predictors used in the GDAS air mass bias correction is:

1. a constant,
2. the scan angle path,
3. the cloud liquid water (CLW) retrieval,
4. the lapse rate integrated over the simulated weighting functions for each observation, and
5. the square of the integrated lapse rate.

The CLW bias correction component has had a significant impact for microwave instruments. As described in Okamoto and Derber (2005), and shown in Figure 2, there is good correlation between the retrieved CLW and the DMSP-15 SSM/I observed minus simulated brightness temperature differences.

The correlation of bias with CLW is seen with other microwave instrument channels; the CLW bias correction component for NOAA-16 AMSU-A channels 1, 2, 3, and 15 is shown in Figure 3. The CLW bias correction is also relatively stable over time. The evolution of the CLW bias correction coefficients for the same channels over the same time period is shown in Figure 4. Again, the coefficients are relatively stable only changing significantly on Nov. 29, compensating for the updates to the fixed angle bias correction in the GDAS.

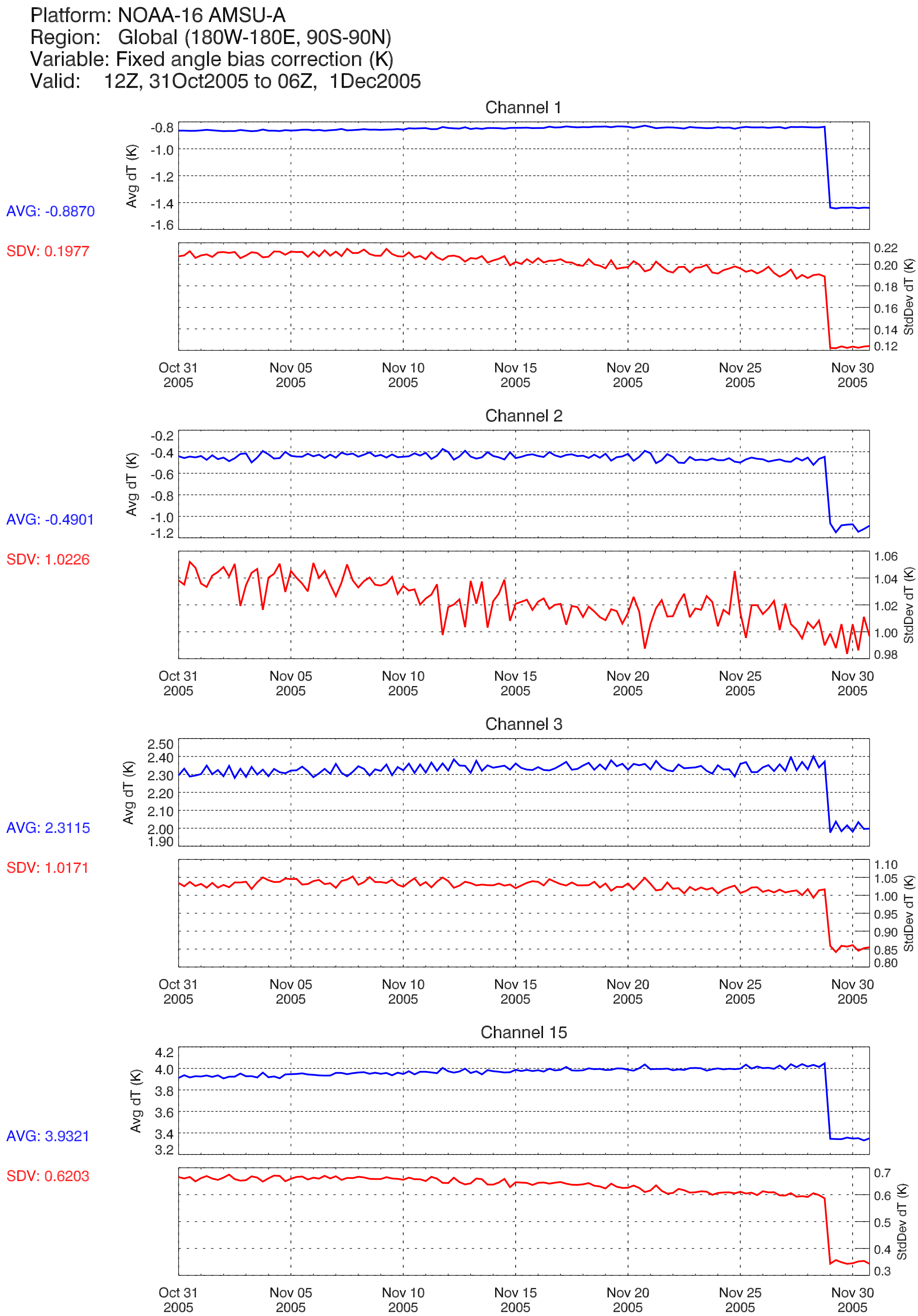

Figure 1 Time series of the average (blue upper plots) and standard deviation (red lower plots) fixed angle bias correction. Data is for NOAA 16 AMSU-A channels 1, 2, 3, and 15 over the whole globe for the month of November 2005. Average and standard deviations listed to the left of each plot are for the time period. The discontinuity on Nov. 29 is due to an update in several aspects of the GDAS, but mainly due to a fixed angle bias correction update. Note the stability of the bias correction statistics both before and after the Nov. 29 GDAS update.

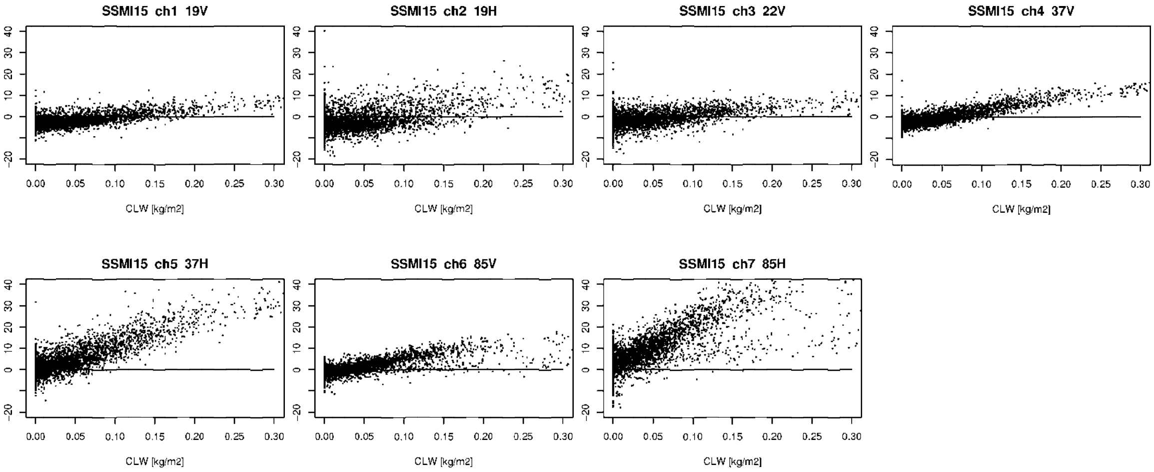

Figure 2 Dependency of observed-minus-guess brightness temperature difference (vertical axis, units are K) on cloud liquid water (CLW, horizontal axis, kg/m2) over the ocean. Data shown is from DMSP-15 SSM/I data after the thinning step at 00UTC on 1 July 2004. From Okamoto and Derber (2005).

Variation of the bias corrected simulated minus observed brightness temperatures, ΔT_B, across a scan are shown in Figure 5 for NOAA-16 AMSU-A. The one-, seven-, and 30-day averages and standard deviations versus scan angle are shown. These plots can indicate whether there is any anomalous behaviour across a scan with respect to time. The ΔT_B averages for each time period typically sit on top of each other, with the standard deviations converging towards the 30-day result. Note that for the time period presented, the one-day standard deviations are lower than the seven- and 30-day values. This is due to the change in the GDAS made on Nov. 29, as is evident from Figure 1.

3. Future investigations

Future research into improving the bias correction applied to simulated satellite radiances in the GDAS can be placed into four categories: a new radiative transfer (RT) model, the profile sets used to train the various components of the RT model, the instrument characterisation, and the methodology used to select predictors in the air mass bias correction scheme.

3.1. New radiative transfer model

The Community Radiative Transfer Model (CRTM) that is currently being integrated into the GSI is a framework of components that are being constructed with the ultimate goal of all-weather data assimilation of satellite radiances. There are four main components of the CRTM which are summarised below. Since the CRTM is still in a state of development, rather than address the potential contributions of each component to any final biases, it should suffice to state that each component (and, where applicable, each different algorithm for any particular component) will have its own unique set of assumptions and biases that will need to be evaluated and corrected for eventual operational use.

3.1.1. Atmospheric absorption

This component handles the absorption of radiation by atmospheric gaseous constituents (e.g. water vapour, ozone, etc). Currently, the atmospheric absorption algorithm used to generate optical depths is a compact version of OPTRAN (Kleespies, *et al*., 2004), but a version of the gaseous absorption component using the Optimal Spectral Sampling (OSS) algorithm (Moncet *et al*., 2004) is also under development. A short description of these two algorithms is shown in Table 1.

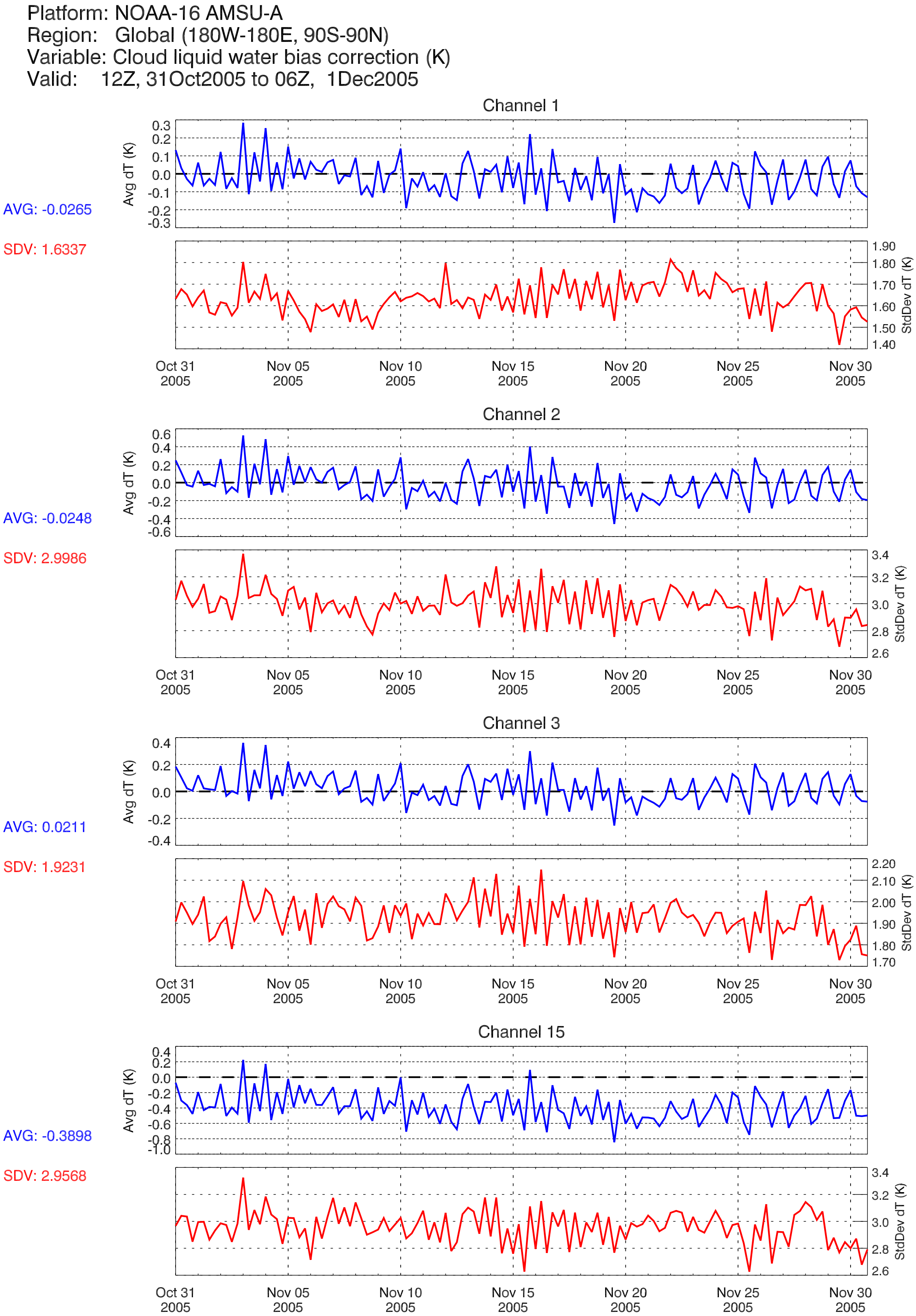

Figure 3 Time series of the average (blue upper plots) and standard deviation (red lower plots) cloud liquid water component of the variational air mass bias correction. Data is for NOAA 16 AMSU-A channels 1, 2, 3, and 15 over the whole globe for the month of November 2005. Average and standard deviations listed to the left of each plot are for the time period.

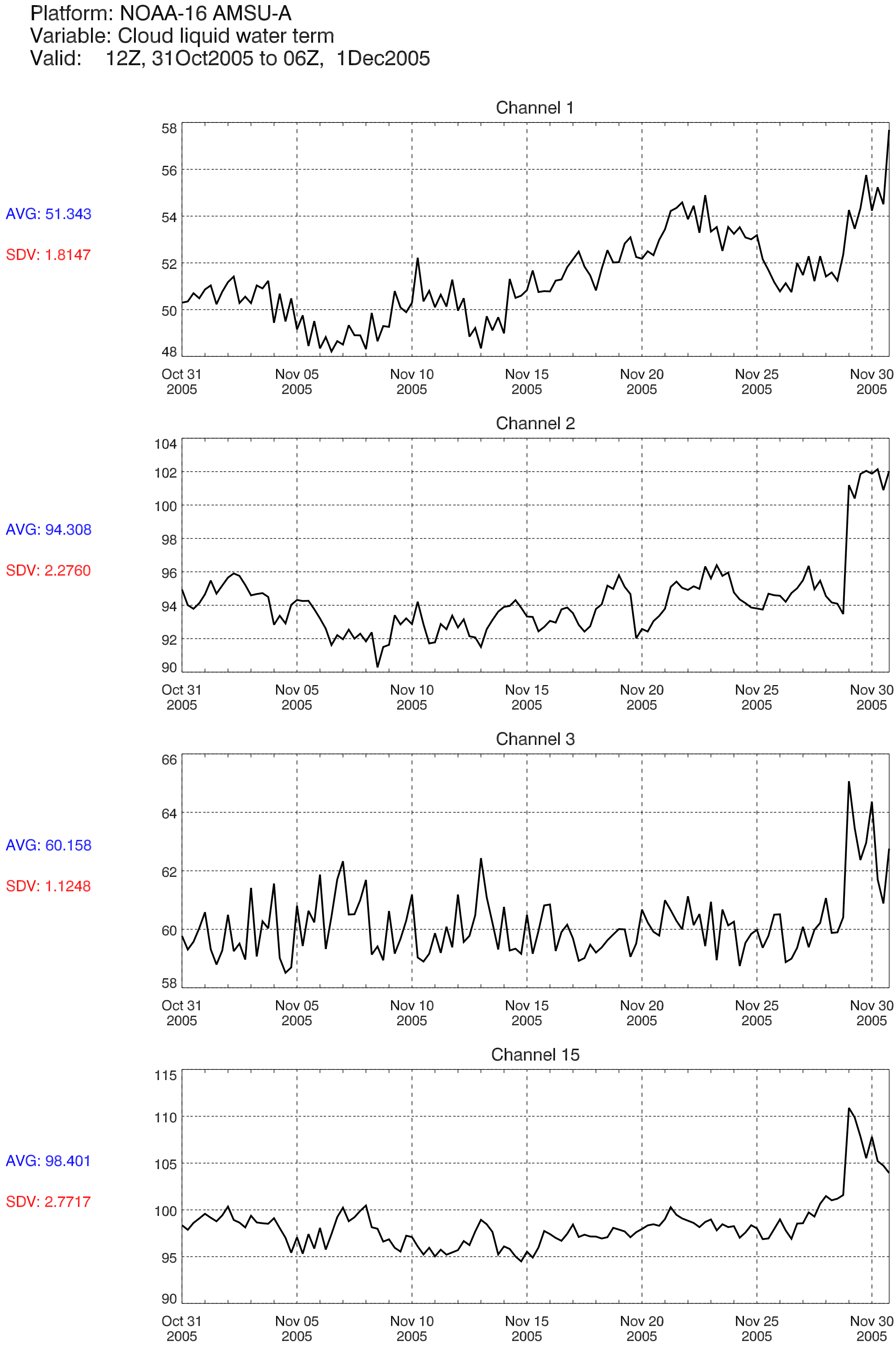

Figure 4 Time series of the coefficients for the cloud liquid water component of the variational air mass bias correction. Data is for NOAA 16 AMSU-A channels 1, 2, 3, and 15 over the whole globe for the month of November 2005. Average and standard deviations listed to the left of each plot are for the time period. The increase seen at Nov. 29 is due to operational changes made in the fixed scan angle bias.

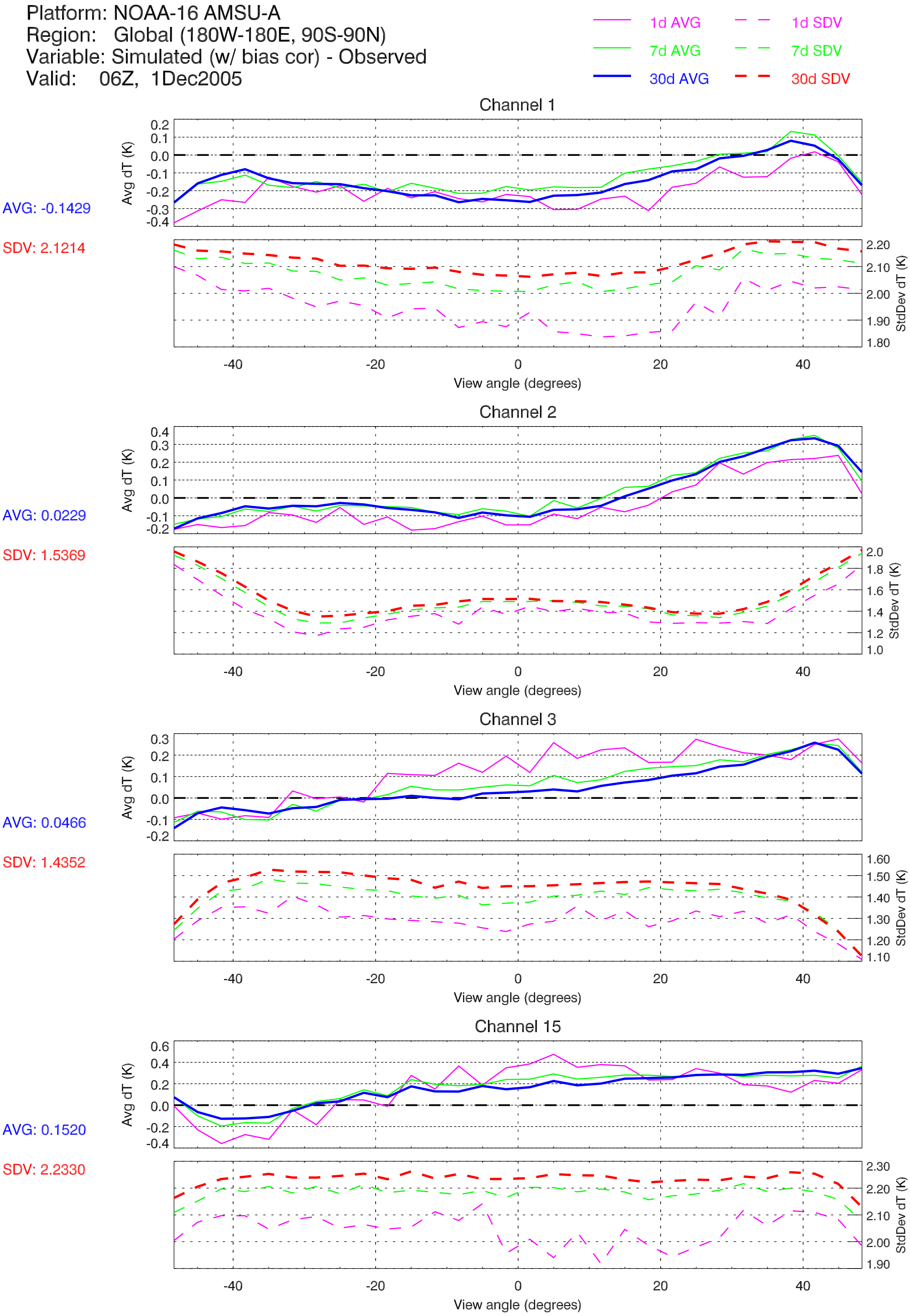

Figure 5 Variation of the average (upper solid line plots) and standard deviation (dashed lower plots) bias corrected simulated minus observed brightness temperatures across a scan. Data is for NOAA 16 AMSU-A channels 1, 2, 3, and 15 over the whole globe for the month of November 2005. Average and standard deviations listed to the left of each plot are for the time period. One, seven, and 30 day statistics are shown.

OPTRAN	OSS
The effective band transmittance for each absorber *j*, T_j, is predicted from the absorption coefficient, ψ, via regression fits, $$\psi_{j,k} = \frac{\log\left(\mathrm{T}_{j,k}/\mathrm{T}_{j,k-1}\right)}{\delta A_{j,k}} = c_{0,k} + \sum_{i=1}^{5} c_{i,j,k} X_{j,k}$$ The selected regression coefficients, c_{ijk}, are those that minimise the transmittance errors. These transmittances are then used in the atmospheric radiative transfer.	Channel radiances are obtained from a weighted sum of monochromatic radiances for a set of predefined nodes, $$\overline{R} = \sum_{n=1}^{N} w_n R_n$$ The monochromatic R_n are obtained from the OSS monochromatic optical depth profiles for the selected node frequencies. Nodes are selected and weights calculated for a channel to satisfy a specified accuracy (e.g. 0.05K). Higher accuracy ⇒ more nodes ⇒ longer computation times.

Table 1. Comparison of the polychromatic OPTRAN and monochromatic OSS algorithms for computing clear sky optical depths/transmittances.

It is expected that the model biases for these two algorithms, particularly for high resolution sensors where residual spectroscopic features still remain in the OPTRAN fits, will be radically different with the assessment of those biases and their subsequent corrections being implementation dependent. The situation becomes even more complex once cloud and aerosol scattering is included. Typical scattering algorithms use nadir optical depths scaled to whatever hemispheric stream angles are required. In the case of OPTRAN, because it is a polychromatic algorithm based on channel resolution transmittances, scaling of optical depths is not mathematically consistent. For OSS, due to the use of predefined nodes, the training process should encompass all the processes for which the atmospheric optical properties are required – otherwise the node selection may not be optimal.

3.1.2. Atmospheric scattering

The atmospheric scattering component of the CRTM is split into two parts: clouds and aerosols. The CRTM is currently set up to handle six different cloud types (water, ice, rain, snow, graupel, and hail) and four different aerosol types (sea salt, organic carbon, black carbon, and sulphates) with four size modes. Because this component of the CRTM is not yet operational, there are no statistics available to assess the bias associated with the scattering and absorption models. In addition, it is not clear whether biases for a particular cloud or aerosol type are similar to those of a different type, particularly – in the case of aerosols – when one also considers different particle size distributions.

3.1.3. Surface optics

The emissivity and reflectivity of different surface types are modeled by the surface optics components of the CRTM. Four different gross surface types (land, ocean, snow, and ice) are modeled separately for each distinct frequency region – currently only microwave and infrared frequencies are supported although visible frequency surface models can be included as they become available. Currently, diffuse and direct reflectivities are determined from the computed emissivities.

3.1.4. Radiative transfer

There are several radiative transfer schemes under consideration for use in the CRTM: fixed multi-stream models (e.g. Liou *et al*., 2005) and flexible-stream models (e.g. Heidinger *et al*., 2005). The selection of a scheme for use in operational use of the CRTM is be dependent on a number of factors such as accuracy, speed, and memory usage, as well as algorithm features such as applicability across frequency regions (e.g. same algorithm for microwave and infrared?) and whether the scheme is fully polarimetric (e.g. full Stokes vector, or just V/H polarisations).

3.2. Profile training sets

3.2.1. Clear sky profile data

Profile sets used in training fast radiative transfer models typically refer to those profiles used to describe the range of gaseous absorbers only, with no cloud or aerosol profile information. In this case, there are still issues to be addressed. At NCEP/EMC, two profile sets are used in training fast radiative transfer models: the UMBC48 and ECMWF52 profile sets, containing 48 and 52 entries respectively of temperature, water vapour and ozone profiles. The UMBC48 set is used to train the NASA-JPL operational AIRS radiative transfer model, and the ECMWF52 set is used to train the ECMWF operational radiative transfer models.

Initially, training of OPTRAN and OSS for use in the CRTM was to be done using the same profile set (UMBC48). However, each model is sensitive to different issues (e.g. OPTRAN has to have absorber overburden in its predictor set due to polychromaticity) and thus have different requirements of the training data. It was found that OPTRAN is better trained using the UMBC48 set (see Figure 6) and OSS using the ECMWF52 set (see Figure 7). It is beyond the scope of this paper to investigate the origin of these differences, but the point needs to be made that the suitability of a training set for an atmospheric absorption algorithm used in a fast radiative transfer model is not necessarily apparent from the results of training other algorithms.

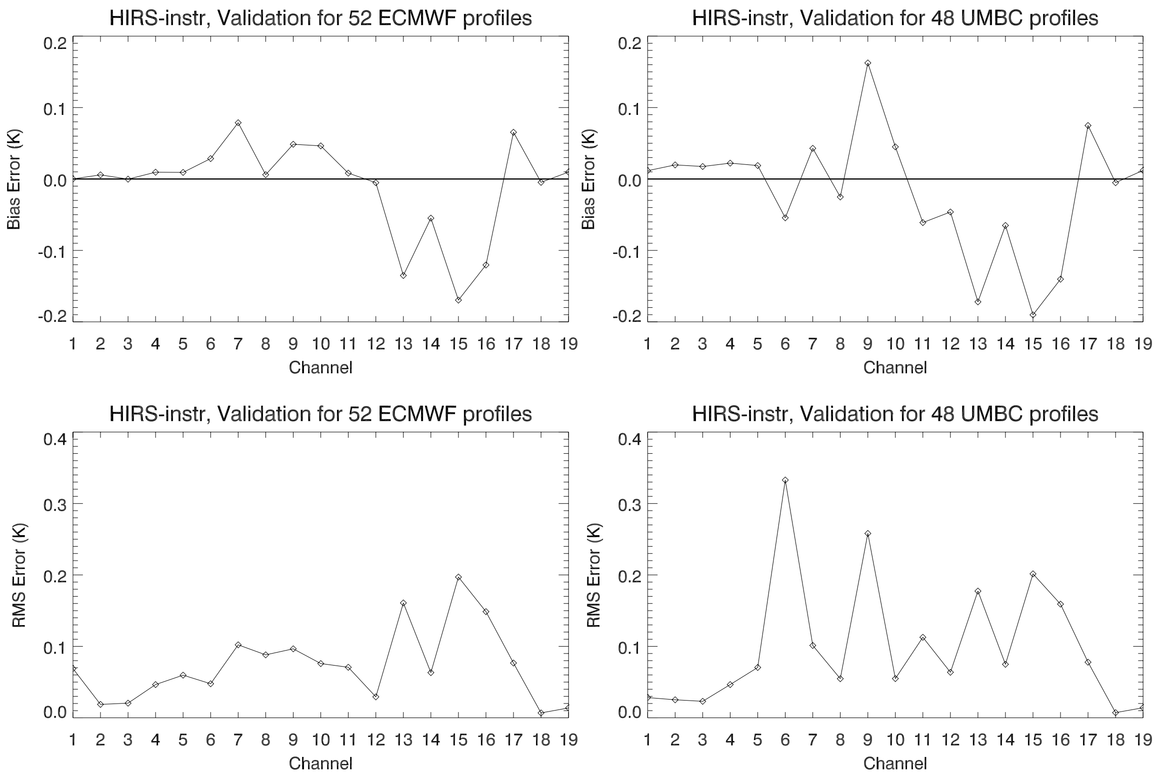

(a) **(b)**

Figure 6 Comparison of statistics for OPTRAN training of HIRS channels. (a) Training with UMBC 48 profiles, validated with ECMWF 52 profiles. (b) Training with ECMWF 52 profiles, validated with UMBC 48 profiles.

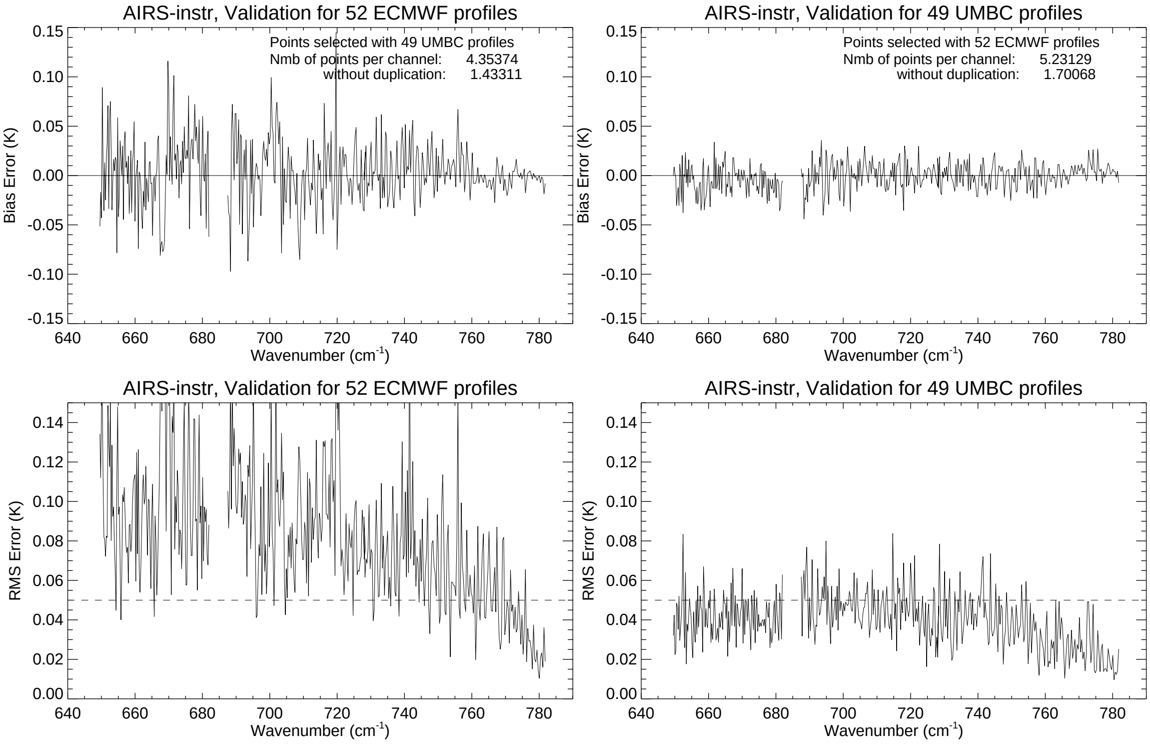

(a) **(b)**

Figure 7 Comparison of statistics for OSS training of AIRS channels. (a) Training with UMBC 48 profiles, validated with ECMWF 52 profiles. (b) Training with ECMWF 52 profiles, validated with UMBC 48 profiles. In both cases the UMBC set was used with its average profile, hence the reference to 49 UMBC profiles. (from J-L. Moncet, AER Inc.)

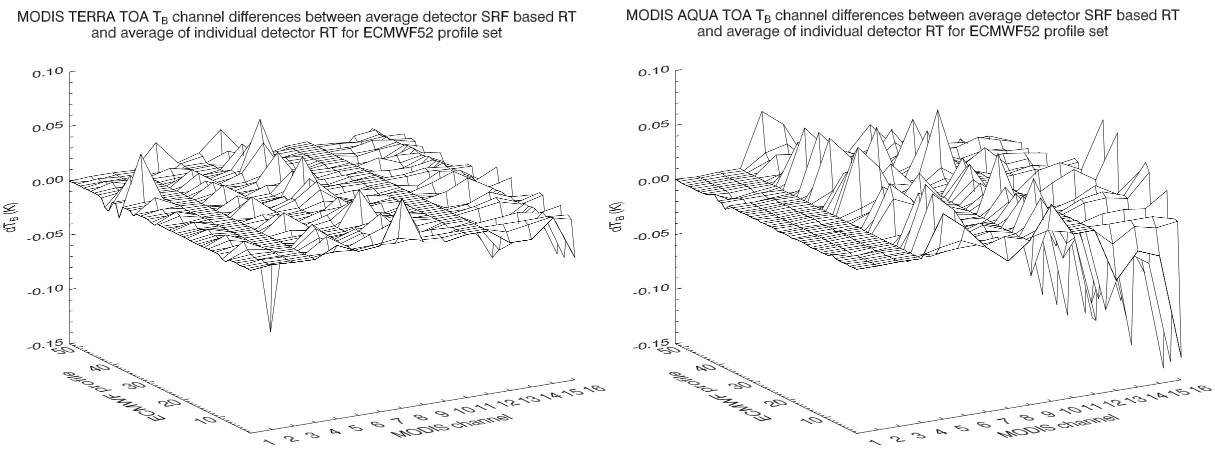

(a) **(b)**

Figure 8 MODIS top-of-atmosphere (TOA) channel brightness temperature differences between radiative transfer results for an average detector SRF (for 10 detectors) and the average of radiative transfer results for the 10 individual detector SRFs. The ECMWF52 profile set was used. (a) MODIS Terra. (b) MODIS Aqua.

3.2.2. Cloud and aerosol profile data

Currently, there is no profile set in hand that characterises the range of cloud and aerosol conditions that will need to be covered in using the CRTM. For an OPTRAN based CRTM – assuming the scaling of polychromatic optical depths can be done correctly – this is less of an issue since the training is done on transmittances directly. The current OSS algorithm, however, trains on radiances so, for optimal selection of monochromatic nodes in both clear sky *and* cloudy or aerosol-laden conditions, the training set must include information about all the physical processes used in the radiative transfer model. Work is being done on the utility of training OSS by transmittances. Regardless of the outcome of that work, the NWP/data assimilation community in general would benefit from a compilation of cloud and aerosol profile data for use in radiative transfer modeling.

3.3. Air mass predictor selection.

The main focus of future investigation into the air mass bias correction is how to optimise the selection of the air mass bias predictors. The current set of predictors, described in §2, do provide significant bias correction, but some preliminary work suggests they are not optimal. Inspection of the various components of the air mass correction indicate that a small bias may be introduced due to the angular dependence of the integrated lapse rate term and, for those affected microwave channels, the cloud liquid water term. A methodology for handling these residual angular dependencies is under development.

3.4. Instrument characterisation

Modeling of instrument channel radiative transfer is almost always channel-based rather than detector-based, and detector differences are typically folded into a mean detector value. This means that any detector array (and thus spectral response function, SRF) differences are not modeled. An example of the effect of this is shown in Figure 8 for the MODIS instrument on EOS Terra and Aqua. The differences are generally small, with some channels performing better than others, and are really only an issue for broadband instruments. Because detector differences are not stable over time, or simply because official SRF measurements may not adequately represent the true instrument response, a variational method of correcting instrument channel characteristics may be useful. This approach would be accompanied by its own set of issues – similar to the variational correction of air mass biases – and it may be simpler to apply and interpret regular offline updates to instrument characteristics.

4. Comments

Research of satellite radiance bias correction schemes at NCEP in the near future will be focused on methods for more optimal selection of the air mass prediction coefficients in the short term, and development of bias correction schemes for new components of the CRTM as it is integrated into the GDAS in the longer term. For the latter work, a comprehensive data set of cloud and aerosol profiles that describe expected amounts and size distributions is needed and will be invaluable in training and validating the CRTM in the GDAS.

5. References

Heidinger, A.K., C.O'Dell, R.Bennartz, and T.Greenwald, 2005, The successive order of interaction radiative transfer model, Part I: Model development, submitted to *Journal of Applied Meteorology*.

Kleespies, T.J., P. van Delst, L.M. McMillin, and J.C.Derber, 2004, Atmospheric transmittance of an absorbing gas. 6. OPTRAN status report and introduction to the NESDIS/NCEP community radiative transfer model, *Applied Optics*, **43**, pp3103-3109.

Liou, K.N., S.C.Ou, Y.Takano, and Q.Liu, 2005, A polarized delta-four-stream approximation for infrared and microwave radiative transfer: Part I, *Journal of the Atmospheric Sciences*, **62**, pp2542-2554.

Moncet, J., G.Uymin, and H.E.Snell, 2004, Atmospheric radiance modeling using the Optimal Spectral Sampling (OSS) method, SPIE Defense and Security Symposium, 13 April 2004, Orlando, Florida: Conference 5425: Algorithms and Technologies for Multispectral, Hyperspectral, and Ultraspectral Imagery X, 5425-37.

Okamoto, K. and J.C.Derber, 2005, Assimilation of SSM/I radiances in the NCEP Global Data Assimilation System, submitted to *Monthly Weather Review*.